Flow process of weak shocks in solids

Duane C. Wallace
Los Alamos Scientific Laboratory, Los Alamos, New Mexico 87545
(Received 17 April 1979)

Experimental measurements of weak-shock profiles in the alloy 6061-*T*6 Al are analyzed by irreversible-thermodynamic finite-strain theory to obtain a complete description of the flow process through the shock compression, including the entropy production and the relations among the flow variables of shear stress, plastic strain, and plastic strain rate. The primary quantities, the normal stress and the normal strain, are determined entirely from the equations of motion and the shock-profile data; the secondary quantities, the shear stress, plastic strain, temperature, and entropy, are then determined by thermodynamics. It is shown that infinitesimal strain theory gives unreliable results as soon as the plastic strain becomes of the same order of magnitude as the elastic strain.

I. INTRODUCTION

A rich source of experimental information on dynamic deformation processes in solids is shock profiles in the weak-shock region[1]; the term *weak shock* is here used to mean a shock whose velocity is not greater than the elastic precursor velocity. The profile measurements are capable of determining the particle velocity as a function of position and time in a solid through which a planar shock is propagating. This gives a one-variable map of the shock-induced deformation process, since the particle velocity is one of the several variables which are coupled into the process. The complete process is governed by three coupled subsets of equations[2]: the equations of motion, which express conservation of mass, momentum, and energy; the thermoelastic equations, which are relation among stresses, elastic strains, temperature, and so on, and whose coefficients are reasonably well known experimentally in the weak-shock region; and the plastic constitutive equation which relates the plastic-flow variables. The plastic constitutive relation is experimentally the least-known material property involved in the whole process. Experimental shock profiles have generally been analyzed by constructing parametrized dislocation models to represent the plastic flow. The decay of the elastic precursor in iron[3] was so analyzed by Taylor[4] and by Rohde,[5] and in aluminum by Arvidsson *et al.*[6] In a series of papers on single-crystal LiF, the Washington State University group developed a model based on nucleation and growth of dislocation loops.[7] A detailed numerical study of dislocation multiplication effects on profile shapes has been carried out by Herrmann and co-workers at Sandia.[8]

In the present work we take an alternative approach: Given the weak-shock profiles and the relevant thermoelastic properties of the solid under consideration, we set out to extract from this information the constitutive relations governing the plastic flow. The results so obtained can be considered experimental results, independent of a dislocation-dynamics theory. A profile analysis of the present kind is made possible by the great increase in experimental precision in recent years, as illustrated by the example of 6061-*T*6 Al: The 1963 measurements of Lundergan and Herrmann,[9] with a time resolution of approximately 2 μs, gave a value of 6.4 ± 0.7 kbar for the Hugoniot elastic limit; the 1969 measurements of Johnson and Barker[10] with resolution of a few ns gave 4.1 kbar.

The Johnson and Barker data are analyzed in the following section, and the flow variables, which are the shear stress, plastic strain, and plastic strain rate, are determined with respectable precision through each shock profile.

II. PROFILE ANALYSIS

A. Shock velocity and particle velocity

We have chosen to study 6061-*T*6 Al because there are available a set of shock profiles and also measurements of the polycrystal third-order elastic constants. The profile data of Johnson and Barker[10] are shown in Fig. 1, in the form of the particle velocity as a function of time t, where $t=0$ when the elastic precursor arrives at the aluminum surface. The measurements were accomplished with a laser velocity interferometer looking at the aluminum through a fused-quartz window; a small impedance-difference correction was applied to transform surface velocity to particle velocity.

The qualitative character of the profiles is illustrated in Fig. 2, where the various states in the shock compression process are lettered, from the initial state a at zero stress and room temperature to the final state e. The experi-

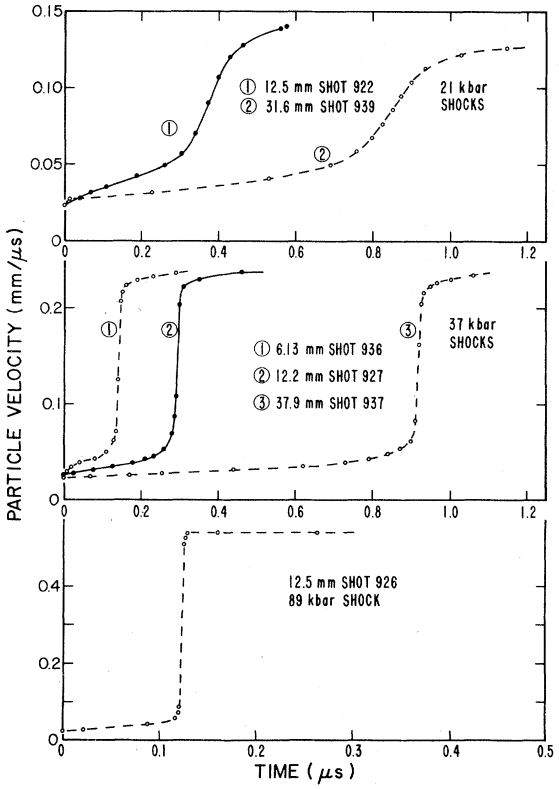

FIG. 1. Data of Johnson and Barker (Ref. 10) for six impact experiments on 6061-*T*6 Al.

ment supports the following description: The front from state a to state b, called the elastic precursor, is a steady wave; the region from state b to state c, which we call the plastic precursor, is nonsteady; the plastic wave from state c to state e is steady with velocity D. We generally refer to D as the shock velocity.

A precision method for measuring all three of the adiabatic polycrystal third-order elastic constants ζ, ξ, ν was described by Clifton.[11] His results for these for 6061-*T*6 Al, and also for the two adiabatic second-order elastic constants λ, μ (the Lamé constants), and for the initial-state density ρ_a, are

$$\rho_a = 2.703 \text{ g/cm}^3, \quad \zeta = -1.40 \text{ Mbar},$$
$$\lambda = 0.544 \text{ Mbar}, \quad \xi = -2.82 \text{ Mbar}, \tag{1}$$
$$\mu = 0.276 \text{ Mbar}, \quad \nu = -4.69 \text{ Mbar}.$$

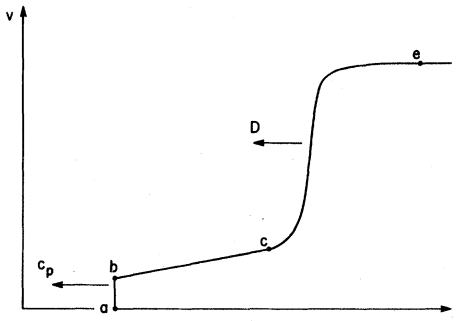

FIG. 2. Schematic representation of a shock profile moving as two steady waves and an intervening unsteady region. Particle velocity v as a function of time t.

The first step in the analysis is to determine the shock velocity for each profile. For the first five shots of Fig. 1 (all but 926), the original data time record runs from impact time; hence it is possible to compute for these shots the elastic precursor velocity c_p (in mm/μs):

$$c_p = 6.46 \pm 0.01, \tag{2}$$

where the ± 0.01 represents merely the experimental scatter. This velocity is considerably faster (1.4% faster) than Clifton's value[11] of the longitudinal sound speed c_l (in mm/μs):

$$c_l = 6.37. \tag{3}$$

The difference is mostly due to finite-strain effects in the elastic precursor: The normal strain on the precursor is $\epsilon_b = 0.0037$ and this is not exactly infinitesimal. With the elastic constants of Eq. (1), I calculate a velocity of 6.43 mm/μs in finite-strain theory for a steady wave of this strain amplitude.

Since the profile analysis is going to be based on the treatment of the plastic wave of each profile as a steady wave, the appropriate velocity D has to be computed from the difference in arrival times of two similar steady waves. This procedure eliminates any nonsteady effects which may have been present in the time immediately following impact. In this way we obtain one velocity from the two shocks at 21 kbar and two independent velocities from the three shocks at 37 kbar. Comparing these results with velocities determined from the arrival time of each separate plastic wave shows small differences (of order 1%) for the 21-kbar shocks and no differences (random scatter of order 0.2%) for the 37 kbar shocks. It is therefore safe to compute the shock velocity for the 89-kbar shock from the precursor velocity (2) together with the profile time record shown in Fig. 1.

A well-established experimental result for shocks up to the Mbar range is that shock velocity is proportional to the final-state particle velocity v_e.[12] In the present work, where one D is computed from two profiles, we assign the corresponding value v_e as the average for the two profiles; there is no averaging for shot 926. The resulting collection of four $D(v_e)$ points is

plotted in Fig. 3, along with the least-squares-fitted straight line

$$D = 5.26 + 1.47 v_e \text{ mm}/\mu\text{s} . \tag{4}$$

Also shown for comparison is the result of Marsh and McQueen[13] for 6061 Al of unspecified hardness; they measured D for shocks of 70 to 680 kbar and fitted the data to the line $D = 5.29 + 1.38 v_e$. The agreement is good in the pressure region of comparison. In the subsequent analysis, we take D from the relation (4).

B. Integration of the equations of motion

The equations for conservation of mass and conservation of linear momentum in plane-wave geometry are given in Ref. 2, Eqs. (40) and (41), in a mixed Eulerian-Lagrangian form; it is convenient here to use the Lagrangian forms

$$\frac{\partial \epsilon}{\partial t} = -\frac{\partial v}{\partial X} , \tag{5}$$

$$\frac{\partial \sigma}{\partial X} = -\rho_a \frac{\partial v}{\partial t} , \tag{6}$$

where X is the Lagrangian coordinate, i.e., the position in the initial configuration of a material plane, $\epsilon = 1 - \rho_a/\rho$ is the normal strain, σ is the normal stress, all variables are functions of X and t, and $v(X, t)$ is the particle velocity, i.e., the velocity in the shock propagation direction of that material plane whose Lagrangian coordinate is X.

We define a steady wave as one which propagates at a fixed velocity without changing its shape; in mathematical terms this means $v(X, t)$ is a function of only one variable, namely $X - ct$, where c is the propagation velocity:

$$v(X, t) = v(X - ct) . \tag{7}$$

If a wave is steady, or if any portion of the wave in a fixed range of the particle velocity is steady, then we can argue that the flow process is steady in that range, i.e., each successive planar slab of material passes along the same physical path while the steady wave passes over the material plane. This means each thermodynamic variable is also a function of only $X - ct$, and in particular

$$\begin{aligned} \epsilon &= \epsilon(X - ct) , \\ \sigma &= \sigma(X - ct) . \end{aligned} \tag{8}$$

Under the conditions (7) and (8), the equations of motion (5) and (6) become the total differential equations

$$d\epsilon = c^{-1} dv , \tag{9}$$

$$d\sigma = \rho_a c\, dv . \tag{10}$$

Equations (5) and (6) can now be integrated through the profile illustrated in Fig. 2, as follows.

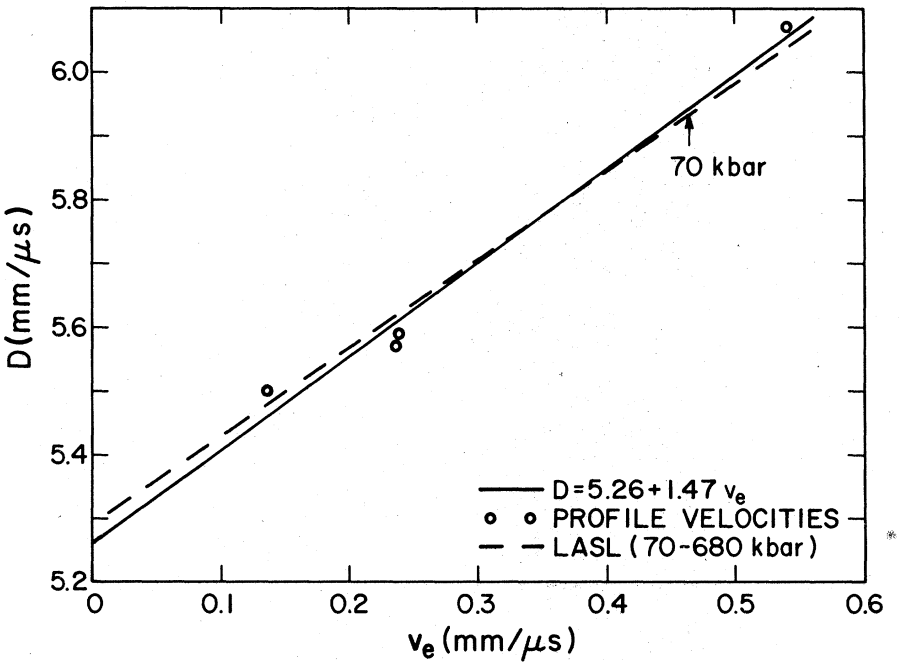

FIG. 3. Shock velocity versus particle velocity for 6061-T6 Al. Data points are from the Johnson and Barker profiles, the straight line is a least-squares fit to these points, the dashed line is the fitted result of Marsh and McQueen (Ref. 13).

Elastic precursor. The front is steady and moves at velocity c_p; the initial conditions are $\epsilon_a = 0$, $\sigma_a = 0$; Eqs. (9) and (10) then give

$$\epsilon_b = v_b/c_p, \tag{11}$$

$$\sigma_b = \rho_a c_p v_b . \tag{12}$$

Plastic precursor. States b and c are characterized by constant values of v_b and v_c moving at the velocities c_p and D, respectively; an approximation compatible with the experimental data for $v(X, t)$ between states b and c is the straight line

$$v = v_b + (v_c - v_b)\left(\frac{c_p t - X}{X\delta}\right), \quad \delta = \frac{c_p - D}{D}. \tag{13}$$

For this function, (5) and (6) integrate to

$$\epsilon = \epsilon_b + \frac{v - v_b}{c_p}\left(1 + \frac{\delta(v - v_b)}{2(v_c - v_b)}\right), \tag{14}$$

$$\sigma = \sigma_b + \rho_a c_p\left(\frac{v_c - v_b}{\delta}\right)\ln\left(1 + \frac{\delta(v - v_b)}{(v_c - v_b)}\right). \tag{15}$$

Plastic wave. We can again use the steady wave forms (9) and (10) to integrate from c toward e and find

$$\epsilon = \epsilon_c + D^{-1}(v - v_c), \tag{16}$$

$$\sigma = \sigma_c + \rho_a D(v - v_c). \tag{17}$$

It may be noted that we have relied heavily on the experimental data in devising the above integration procedure. For the six profiles of Fig. 1, v_b lies in the range 0.023–0.026 mm/μs, with nothing in the data to indicate a dependence on either the shock strength or the propagation distance. As for the value of v_c, this can be chosen somewhat arbitrarily, but all the profiles are consistent with $v_c = 0.050$ mm/μs, which was used in the present calculations. For the $v(X, t)$ curve in the unsteady region from b to c, we are fortunate that experiment provides a simple analytic approximation. This also allows us to see clearly a result which may be expected to hold in general: For the unsteady flow region, the Rayleigh line, which is the $\sigma(\epsilon)$ relation, is not a straight line. The Rayleigh line is straight for a steady wave; this is obvious from the combination of Eqs. (9) and (10) to give $d\sigma = \rho_a c^2 d\epsilon$. But for σ and ϵ on the plastic precursor, the combination of (14) and (15) produces a $\sigma(\epsilon)$ relation which is slightly curved (concave downward) in this region.

We used the above equations to calculate σ and ϵ as functions of v for each of the six profiles. The raw data points for v were used. The results for the two profiles at 21 kbar, and for the three at 37 kbar are in excellent internal agreement.

C. The flow behavior

The thermoelastic differential equations for the normal stress σ and the shear stress τ for plane-wave geometry are given in Ref. 2, Eqs. (37) and (38). The independent strain variables are the total normal strain ϵ and the plastic strain ψ. Since the strains are small in weak shocks, it is convenient here to integrate $d\sigma$, $d\tau$ and express σ, τ as power series in ϵ, ψ. This can be done in either of the following two ways: (a) Expand the stress-strain coefficients in powers of elastic strains, convert to ϵ, ψ, and integrate $d\sigma$, $d\tau$ or (b) expand the internal energy in powers of elastic strains and calculate stresses from their thermoelastic definition as strain derivatives of the internal energy.[14,15] We carry the expansion of σ, τ only to second order in strains because coefficients of third-order terms involve the fourth-order elastic constants, whose values we do not know.

In addition to the strain terms, the equations for $d\sigma$, $d\tau$ contain the following terms in the entropy: $\rho\gamma_1 T dS$ in $d\sigma$ and $\frac{1}{2}\rho(\gamma_1 - \gamma_2)T dS$ in $d\tau$, where T is the temperature, S is the entropy per unit mass, and γ_β are the anisotropic Grüneisen parameters. Since $T dS$ is proportional to $\tau d\psi$,[2] and since τ is of lowest-order linear in strains, $T dS$ is a second-order quantity. Hence to express the above $T dS$ terms correct to second order, γ_β may be evaluated to lowest order in strains, which means γ_β may be taken as the ordinary Grüneisen parameter evaluated in the initial state γ_a. The completed results for σ and τ to second order in strains are

$$\begin{aligned}\sigma = {} & (\lambda + 2\mu)\epsilon - 2\mu\psi - (\tfrac{3}{2}\lambda + 3\mu + \zeta + 2\xi)\epsilon^2 \\ & + (4\lambda + 10\mu + 4\xi)\epsilon\psi - (\tfrac{3}{2}\lambda + 6\mu + \tfrac{3}{2}\xi + \tfrac{1}{4}\nu)\psi^2 \\ & + 2\gamma_a \int_0^{\epsilon,\psi} \tau(\epsilon', \psi')d\psi' ,\end{aligned} \tag{18}$$

$$\begin{aligned}\tau = {} & \mu(\epsilon - \tfrac{3}{2}\psi) - (\lambda + \tfrac{3}{2}\mu + \xi)\epsilon^2 \\ & + (\tfrac{3}{2}\lambda + \tfrac{9}{2}\mu + \tfrac{3}{2}\xi + \tfrac{1}{4}\nu)\epsilon\psi - (\tfrac{9}{4}\mu + \tfrac{3}{8}\nu)\psi^2 .\end{aligned} \tag{19}$$

The integral in (18) is the entropy contribution to σ; an entropy contribution to τ would appear in third order.

By integrating the equations of motion, we have already determined the variables σ, ϵ through each shock profile; note for a given profile the variables correspond to a fixed Lagrangian coordinate, i.e., to a fixed planar slab of material. With σ, ϵ given, Eqs. (18) and (19) were then solved for τ, ψ. Because of the $\int \tau d\psi$ in (18), it was necessary to solve (18) and (19) simultaneously by numerical iteration. For γ_a, we used the value for pure aluminum,[14]

$$\gamma_a = 2.16 . \qquad (20)$$

The results for τ as a function of ψ through each shock profile are shown in Figs. 4–6. Since the time variable through each profile is also known from experiment, it is possible to calculate $\dot{\psi}$, the Lagrangian time derivative of ψ. These results are also shown in Figs. 4–6. The shaded area at the top of each $\dot{\psi}$ curve is meant to indicate the experimental scatter there; this scatter is not significant in the overall analysis since we have $\dot{\psi}$ spanning a range of four orders of magnitude.

It is seen from Figs. 4–6 that the shear stress increases rapidly, and drives up the flow rate, at the beginning of the flow process; toward the end of the process the plastic flow slows, and it finally stops when the material reaches the static state e, where ψ reaches its maximum. For the 89-kbar shock the rise of the plastic wave was possibly too fast to be followed by the instrumentation, so the observed rise time of 5 ns is an upper limit (see Fig. 1); therefore the maximum plastic strain rate of 10^7 s^{-1} in Fig. 6 may be only a lower limit. The flow curves of Figs. 4–6 support two qualitative conclusions for 6061-$T6$ Al, as follows:

(a) The rapid increase of the shear stress at the flow front is due mainly to strain-rate effects.

(b) Except for possibly the weakest shocks, the shear stress decreases in the approach to static equilibrium behind the shock.

We comment now on the errors in the τ, ψ curves. At the front of each curve the error in τ is small since the total strain there is mostly elastic. Later, however, τ no longer increases even though ϵ continues to increase strongly. This is because the metal is flowing in such a way as to keep the shear stress from increasing, i.e., plastic flow is canceling out much of the increase in the anisotropic part of the purely

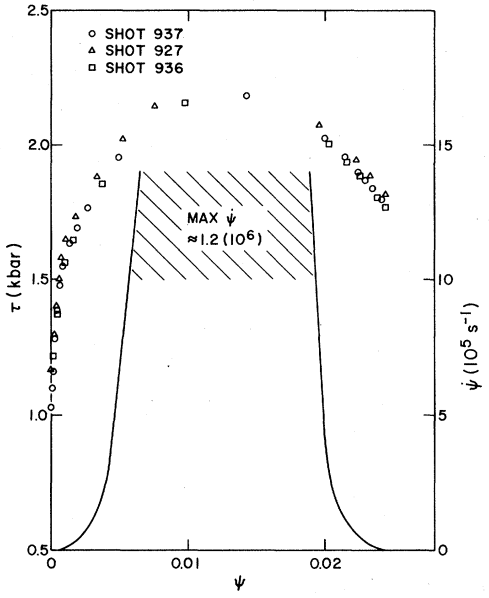

FIG. 5. Plastic-flow process for three shocks at 37 kbar.

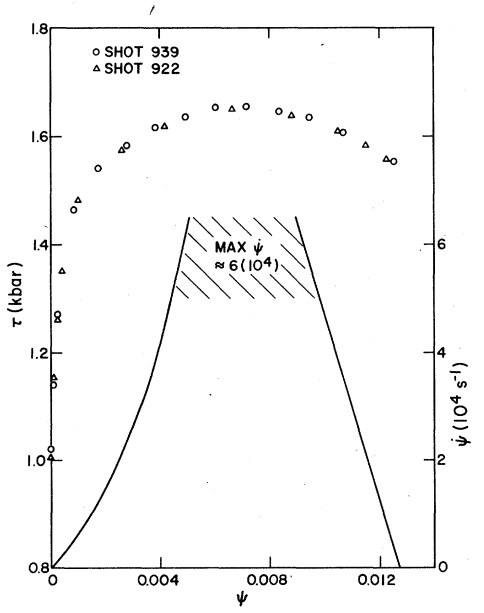

FIG. 4. Plastic-flow process for two shocks at 21 kbar.

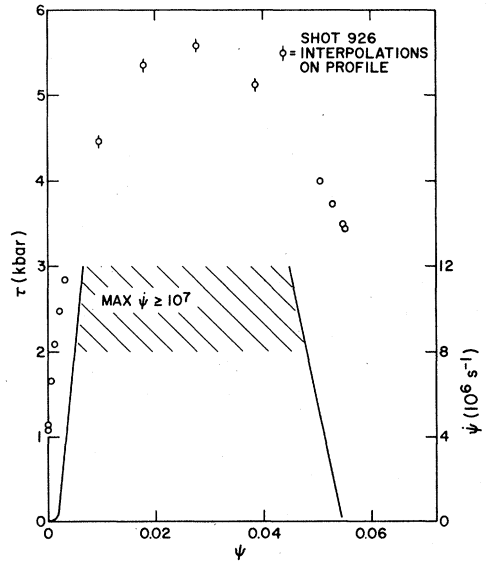

FIG. 6. Plastic-flow process for the 89-kbar shock. The four points indicated were interpolated as a straight line in particle velocity versus time on the plastic wave front (see Fig. 1).

elastic strain. Because of this subtle cancellation, the error in our computed τ, which comes ultimately from errors in our thermoelastic stress-strain relations, can be significant in the late stage of each shock compression profile (near the final state). The effect depends in a complicated way on the coupling between the equations for ψ and τ. To learn something about this we computed ψ and τ at the final state in infinitesimal strain theory; that is, from equations (18) and (19) with the second-order strain terms omitted. The results are compared with the second-order calculations in Table I. It is seen that infinitesimal strain theory produces unacceptable results for all the shock groups. It is further obvious that inclusion of the next-higher-order strain terms, corresponding to fourth-order elastic constants, would be desirable for the 89-kbar shock.

D. Constitutive relations

In addition to the steady-wave profiles analyzed above, Johnson and Barker[10] also presented a series of 9.5-kbar profiles which show the decay of the elastic precursor through a material distance X of 4 to 38 mm. In these experiments they measured the free surface velocity, which gives quite accurately the particle velocity at the profile point b through the relation: v_b equals half the free surface velocity at b. These data can be analyzed by Taylor's theory,[4] which is based on the observations that the elastic precursor travels on the lead C_+ characteristic and that $\psi=0$ there. With the characteristic velocity c_p, the equations of Ref. 4 give

$$\psi_b = 0\,, \qquad \dot{\psi}_b = -\frac{\rho_a c_p^2}{\mu}\frac{dv_b}{dX}\,. \tag{21}$$

From this and (19), the shear stress is

$$\tau_b = \mu\epsilon_b - (\lambda + \tfrac{3}{2}\mu + \xi)\epsilon_b^2\,, \tag{22}$$

where ϵ_b is given in leading order by (11). Thus from the elastic precursor data for $v_b(X)$, we can find the $\tau, \dot{\psi}$ relation on the line $\psi=0$.

TABLE I. Final-state values ψ_e, τ_e as calculated in infinitesimal strain theory and in second-order theory, averaged for each shock group. Also the entropy contributions to ψ_e, τ_e. τ_e is in kbar.

Shock group (kbar)	Infinitesimal ψ_e	Infinitesimal τ_e	Second order ψ_e	Second order τ_e	Entropy contribution ψ_e	Entropy contribution τ_e
21	0.010	2.6	0.013	1.6	1%	−4%
37	0.016	5	0.024	1.8	1%	−9%
89	0.016	18	0.055	3.5	3%	−25%

The flow relations we have determined are shown in Fig. 7 as curves of τ vs $\dot{\psi}$ at fixed ψ. The $\psi=0$ curve is from the elastic precursor decay, Eqs. (21) and (22). The curves for $\psi = 0.001, 0.002, 0.004$ are each composed of three points; one from the 21-kbar shocks (Fig. 4), one from the 37-kbar shocks (Fig. 5), and one from the 89-kbar shock (Fig. 6). Though the values of ψ are very small, all of these curves are quite accurate; recall that cancellation errors in τ are not important when ψ is small. A set of points at the largest plastic strains we could determine were taken from near the end of the 89-kbar shock; these have ψ values of 0.048–0.054, and we expect them to be accurate in ψ and $\dot{\psi}$ but possibly in significant error in τ. It should also be noted that these points represent material under a pressure of approximately 84 kbar and at a temperature of about 380 K. Results reported recently by Herrmann,[16] based on analysis of part of the same experimental data through a relaxation function formalism, differ significantly from the present results, presumably due to the inclusion here of third-order elastic constants and entropy effects (the two methods are compared analytically in Ref. 2). The plastic-flow behavior of 6061-$T6$ Al was measured by Holt *et al.*[17] for ψ up to 0.08 and $\dot{\psi}$ from 10^{-3} to 10^{3} s^{-1}; they observed essentially no strain-rate dependence at all, and a mild strain hardening. The curves of Fig. 7, extrapolated to low strain rates, are consistent with the measurements of Holt *et al.* Note that in the extrapolation to low strain rates, the four curves for small ψ values will all cross, giving τ as an increasing function of ψ at a fixed $\dot{\psi}$ of say $\dot{\psi}=10^{3}$ s^{-1}.

E. Temperature and entropy

The theory of Ref. 2 also enables us to calculate the temperature and entropy through the shock profiles by means of the equations

$$T\,dS = 2V\tau\,d\psi\,, \tag{23}$$

$$T\,dS = C_\eta[dT + T\gamma_1 d\ln(1-\epsilon) + T(\gamma_1-\gamma_2)d\psi]\,, \tag{24}$$

where $V=\rho^{-1}$ is the volume per unit mass and C_η is the heat capacity at constant elastic configuration. The anisotropic Grüneisen parameters may be expressed as derivatives of the stresses τ_β with respect to the internal energy U at constant elastic configuration[2,14]:

$$\rho\gamma_\beta = -\left(\frac{\partial\tau_\beta}{\partial U}\right)_\eta\,. \tag{25}$$

A set of approximations which simplify the numerical integration of (23) and (24), and which

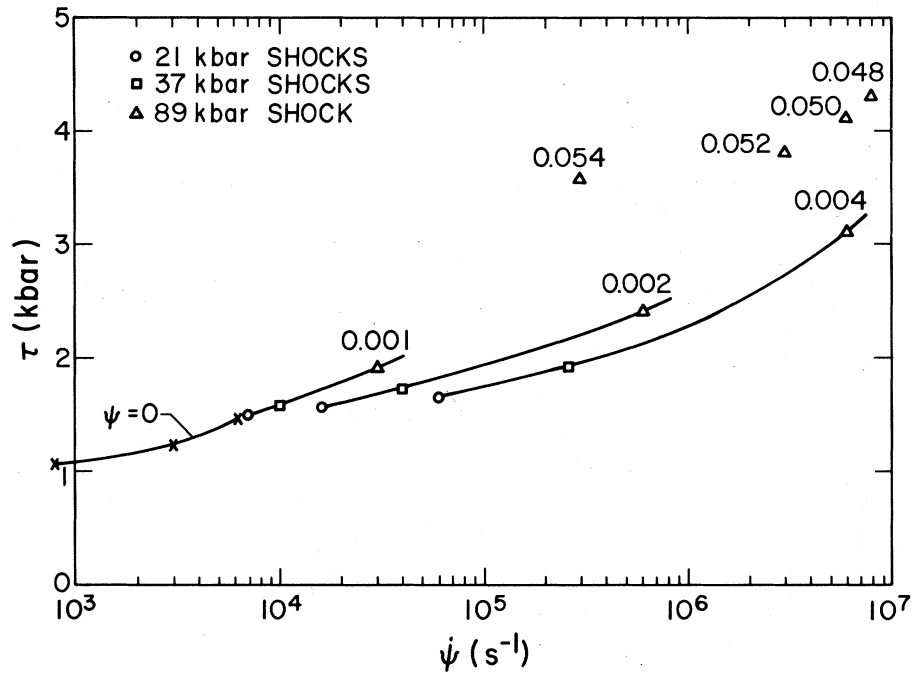

FIG. 7. Shear stress τ as a function of plastic strain rate $\dot{\psi}$ for lines of constant ψ. The numbers label the value of ψ for the lines and points.

are of acceptable accuracy for the present calculations, are

$$\begin{aligned} &\gamma_1=\gamma_2=\gamma, \\ &C_\eta=C_V, \\ &C_V=0.88\times10^7, \\ &\rho\gamma=\text{constant}=\rho_a\gamma_a, \end{aligned} \tag{26}$$

where the C_V for 6061-T6 Al is measured in erg/gm K. The first approximation expresses the idea that the thermal energy exerts outward forces in an essentially isotropic way, i.e., it contributes nearly equally to all three principal stresses [see Eq. (25)]. $C_\eta=C_V$ is the same sort of approximation. To support taking C_V constant, we note that for any characteristic temperature theory, as e.g., the Debye theory, with characteristic temperature Θ a function only of the volume, the relations hold:

$$S=S(\Theta/T), \quad \Theta=\Theta(V);$$

then $S=$ constant implies $\Theta/T=$ constant, which implies $C_V=$ constant. Since entropy generation is small in the weak-shock region, the thermodynamic states are not far from $S=S_a$, and C_V is not far from its value in the initial state, which is the value given for 6061-T6 Al in (26). Finally the approximation $\rho\gamma=$ constant is in keeping with $d\ln\gamma/d\ln V\approx-1$ for pure Al,[14] and with the extensive shock-related study of Neal[18] for Al and Al alloys for compressions up to a factor of 2.

The initial temperature for our calculations was taken as $T_a=295$ K. The values of T and $S-S_a$ in the final state, along with stresses and strains at some intermediate profile points, are listed for each shock group in Table II.

III. DISCUSSION

The application of the general thermoelastic–plastic-flow theory to accurate one-dimensional strain experiments on 6061-T6 Al has been shown to be relatively simple. With the velocity profiles

TABLE II. Thermodynamic quantities at state b and at the final state e. Averages are listed for each shock group. Stress is in kbar, temperature in K, entropy in 10^5 erg/gm K. $T_a=295$ K. The number in parentheses is the last significant digit.

Quantity	21 kbar	37 kbar	89 kbar
ϵ_b	0.0036	0.0038	0.0038
σ_b	4.0	4.1	4.1
τ_b	1.0	1.0(6)	1.0(6)
ϵ_e	0.0240	0.0414	0.089
σ_e	21.0	36.7	89
ψ_e	0.0127	0.0244	0.055
τ_e	1.6	1.8	3.5
T_e	313	327	380
S_e-S_a	0.5	1.2	5.3

divided into steady and self-similar parts in the stress range 20–90 kbar, only algebraic computations are required. For more general profiles the analysis will be more complicated. A more complex space- and time-dependent representation of material velocities is required for the initial evolution of shock profiles, as illustrated by the data of Johnson and Barker[10] at approximately 9 kbar.

Lipkin and Asay[19] have recently reported velocity measurements on 6061-T651 Al at 20 kbar which are approximately self-similar throughout, implying a very weak flow-rate dependence for τ. The present analysis also shows a small strain-rate dependence at the 21-kbar stress level (Figs. 4 and 7). In addition, Asay and Lipkin[20] used the same reshock and release measurements to estimate the shear stress for 6061-T651 Al in the shocked state at 20 kbar. Their result for $Y=2\tau$ is 2.6 kbar; the present result from Fig. 4 at 21 kbar is $2\tau=3.1$ kbar. The difference is not unreasonable in view of uncertainties in either analysis. A new experimental method for propagating large one-dimensional shear waves at high stresses[21] should provide valuable new data for improving our knowledge of the flow functions of metals.

ACKNOWLEDGMENT

I am grateful to Jim Johnson for providing me with his original data notebook from which to work.

[1]J. W. Taylor, in *Dislocation Dynamics*, edited by A. R. Rosenfield *et al.* (McGraw-Hill, New York, 1968), p. 573.
[2]D. C. Wallace, Phys. Rev. B 22, 1477 (1980) (preceding paper).
[3]J. W. Taylor and M. H. Rice, J. Appl. Phys. 34, 364 (1963).
[4]J. W. Taylor, J. Appl. Phys. 36, 3146 (1965).
[5]R. W. Rohde, Acta Metall. 17, 353 (1969).
[6]T. E. Arvidsson, Y. M. Gupta, and G. E. Duvall, J. Appl. Phys. 46, 4474 (1975).
[7]Y. M. Gupta, G. E. Duvall, and G. R. Fowles, J. Appl. Phys. 46, 532 (1975); J. R. Asay, D. L. Hicks, and D. B. Holdridge, *ibid.* 46, 4316 (1975).
[8]W. Herrmann, D. L. Hicks, and E. G. Young, in *Shock Waves and the Mechanical Properties of Solids*, edited by J. J. Burke and V. Weiss (Syracuse University Press, Syracuse, 1971), p. 23.
[9]C. D. Lundergan and W. Herrmann, J. Appl. Phys. 34, 2046 (1963).
[10]J. N. Johnson and L. M. Barker, J. Appl. Phys. 40, 4321 (1969).
[11]R. J. Clifton, in *Shock Waves and the Mechanical Properties of Solids*, edited by J. J. Burke and V. Weiss (Syracuse University Press, Syracuse, 1971), p. 73.
[12]R. G. McQueen, S. P. Marsh, J. W. Taylor, J. N. Fritz, and W. J. Carter, in *High Velocity Impact Phenomena*, edited by R. Kinslow (Academic, New York, 1970), p. 293.
[13]S. P. Marsh and R. G. McQueen, Los Alamos Scientific Laboratory (LASL) file data (unpublished). An updated shock velocity-particle relation for 6061 Al is $D=5.35+1.34v_e$ (LASL Shock Hugoniot Data, University of California Press, Berkeley, 1980).
[14]D. C. Wallace, *Thermodynamics of Crystals* (Wiley, New York, 1972).
[15]D. C. Wallace, in *Solid State Physics*, edited by H. Ehrenreich, F. Seitz, and D. Turnbull (Academic, New York, 1970), Vol. 25, p. 301.
[16]W. Herrmann, in *Propagation of Shock Waves in Solids*, edited by E. Varley (ASME, New York, 1976), p. 1.
[17]D. L. Holt, S. G. Babcock, S. J. Green, and C. J. Maiden, Trans. Am. Soc. Met. 60, 152 (1967).
[18]T. Neal, Phys. Rev. B 14, 5172 (1976).
[19]J. Lipkin and J. R. Asay, J. Appl. Phys. 48, 182 (1977).
[20]J. R. Asay and J. Lipkin, J. Appl. Phys. 49, 4242 (1978).
[21]A. S. Abou-Sayed and R. J. Clifton, J. Appl. Mech. 44, 79 (1979); 44, 85 (1979).